

## Digital Terrain Models from Radar Interferometry

RICHARD BAMLER, Wessling

### ABSTRACT

Interferometric synthetic aperture radar (InSAR) is a rapidly evolving technology for DTM generation. It exploits the coherent nature of SAR imaging to measure stereo parallaxes in the mm and cm regime from phase differences. InSAR systems are active microwave sensors; they operate independent of cloud cover and sun illumination.

This paper reviews the basic principle and the properties of spaceborne SAR interferometers. It is shown how height accuracy and resolution depend on system parameters and temporal decorrelation behaviour of the imaged terrain. A brief overview of current and future SAR and InSAR systems is given.

### 1. INTRODUCTION

With the launch of NASA's satellite SEASAT in 1978 spaceborne imaging radars began to play an important role in Earth remote sensing. It was demonstrated by the early missions that Synthetic Aperture Radar (SAR) is able to reliably map the Earth's surface and acquire information about their physical properties, such as topography, morphology, roughness, and the dielectric characteristics of the backscattering layer. SAR can be most beneficially used over land, ice and sea surfaces. As the spaceborne SAR systems operate in the microwave (cm to dm wavelength) regime of the spectrum and provide their own illumination they can acquire information globally and almost independently of meteorological conditions and sun illumination. This can be a deciding factor when it comes to imaging polar or tropical regions. SARs are, therefore, most suitable for operational monitoring tasks. The side-looking imaging geometry, pulse compression techniques as well as the synthetic aperture concept are employed to achieve resolutions in the order of some metres to tens of metres with physical antennas of modest size. The prize to pay for such favourable performance are high transmit power, enormous amount of signal processing, and - compared to optical imagery - 'unconventional' imaging geometry. For more information on SAR systems and SAR data processing see, e.g. Bamler and Schättler (1993), Curlander and McDonough (1991), Elachi (1991), Harger (1970), Raney (1982a), Raney (1982b), Tomiyasu (1978).

The use of spaceborne SARs as interferometers (interferometric SAR = *InSAR* or *IFSAR*) became popular only recently, although the basic principle dates back to the early 70's as well ((Graham, 1974), (Richman, 1971)). However, concerning terrestrial applications it was only in the 80's that the first results were published ((Gabriel and Goldstein, 1988), (Prati et al., 1989), (Zebker and Goldstein, 1986)). At that time but few SAR data sets were at hand for interferometric investigations.

Only after the launch of the ESA satellite ERS-1 in 1991 an enormous amount of SAR data suitable for interferometry became available and a series of research groups began to investigate the method intensively and with success, to name only a few: Gatelli et al. (1994), Hartl et al. (1993), Hartl et al. (1994a), Hartl et al. (1994b), Lanari et al. (1996), Massonnet et al. (1995), Massonnet and Rabaut (1993), Massonnet et al. (1993), Moreira et al. (1995), Prati and Rocca (1992), Prati and Rocca (1993), Prati et al. (1994), Rodriguez and Martin (1992), Wegmüller and Werner (1997), Wegmüller et al. (1995), Zebker and Rosen (1994), Zebker and Villasenor (1992), Zebker et al. (1994). Today it is generally appreciated that InSAR and the differential InSAR method (*D-InSAR*) are extremely powerful tools for mapping the Earth's land, ice and even the sea surface topography, for detection and mapping of surface displacements over large temporal and spatial scales with precision in the cm- and even mm- range (which is of importance for earthquake and volcanic research), for glaciology and ice sheet monitoring, for study of tectonic processes, for monitoring of land subsidence

due to mining, gas, water, and oil withdrawal, etc., for detection and mapping of dielectric properties of the land surface by making use of the temporal and spatial coherence characteristics allowing for land cover classification, mapping of flooded areas, monitoring of geophysical parameters, etc.

## 2. SYNTHETIC APERTURE RADAR

A synthetic aperture radar (SAR) illuminates the Earth's surface by microwave pulses, i.e. short packages of sine waves, in a side-looking fashion (Figure 1). The received echo signals are recorded with respect to both their magnitude and their phase. Phase denotes the relative shift of the received sine wave with respect to the transmitted one; a full sine wave cycle corresponds to a phase of  $2\pi$ , or 360 degrees. The ensemble of these echoes forms a microwave hologram of the object rather than a sharp image. In a subsequent digital signal processing procedure some hundreds or even thousands of consecutive echoes each are correlated in a way as to focus a highly resolved image of the object. SAR processing can be viewed as simulating - or synthesising - an antenna aperture as large as 100 m - 10 km.

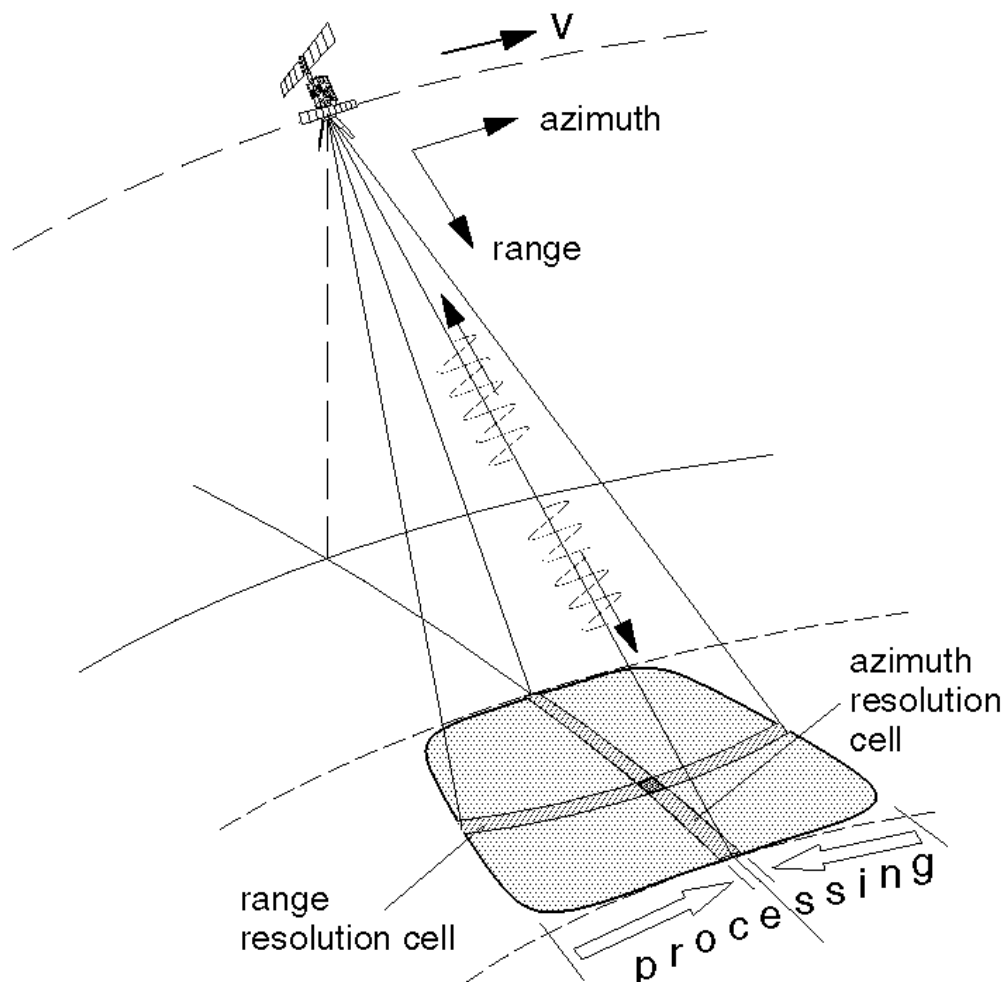


Figure 1: Spaceborne SAR imaging geometry.

Typical resolutions of remote sensing spaceborne SARs are 10 m - 100 m. However, sub-metre resolution is possible. Commonly used wavelengths are 3 cm (X-band), 5 cm (C-band), and 25 cm (L-band).

The SAR imaging process maps the 3-D object, e.g. the Earth's surface, into the 2-D radar co-ordinates *range* and *azimuth*. Range is the distance from a point on the Earth to the SAR sensor and azimuth

represents the sensor's position along its flight path. This type of geometry makes SAR images of mountainous terrain 'look' different or distorted compared to optical images.

The magnitude (brightness) of a pixel in the SAR image is a measure of the object's capability to scatter microwaves. The phase of a pixel carries information both about the phase shift of the scattering mechanism and the delay experienced by the wave propagating from the sensor to the object and back:

$$\phi = \phi_{scatt} + \phi_{prop}$$

The propagation induced phase is a highly sensitive measure for range  $R$ :

$$\phi_{prop} = \frac{4\pi}{\lambda}R$$

where  $\lambda$  is the radar wavelength. Of course,  $\phi$  can only be measured modulo  $2\pi$ .

### 3. SAR INTERFEROMETRY (InSAR)

As with conventional (optical) mapping, terrain reconstruction can be achieved using stereo methods applied to SAR images taken from different orbits. SAR interferometry exploits the phase of SAR signals to measure stereo parallaxes to an accuracy of a fraction of a wavelength, i.e. down to some 1/1000 of a resolution cell. To this end the phase difference of two complex-valued SAR images of the same area, but taken from slightly different orbits, are computed on a pixel-by-pixel basis. Considering the InSAR configuration of Figure 2 the phase difference (or: *interferometric phase*) is found as

$$\Delta\phi = \phi_2 - \phi_1 = \phi_{prop,2} - \phi_{prop,1} = \frac{4\pi}{\lambda}(R_2 - R_1)$$

where the scattering phase is assumed to be invariant, i.e.  $\phi_{pscatt 1} = \phi_{scatt 2}$ . Obviously, the range parallax  $\Delta R = (R_2 - R_1)$  is a measure for the look angle  $\theta$  which, in turn, depends on the terrain height  $h$ .

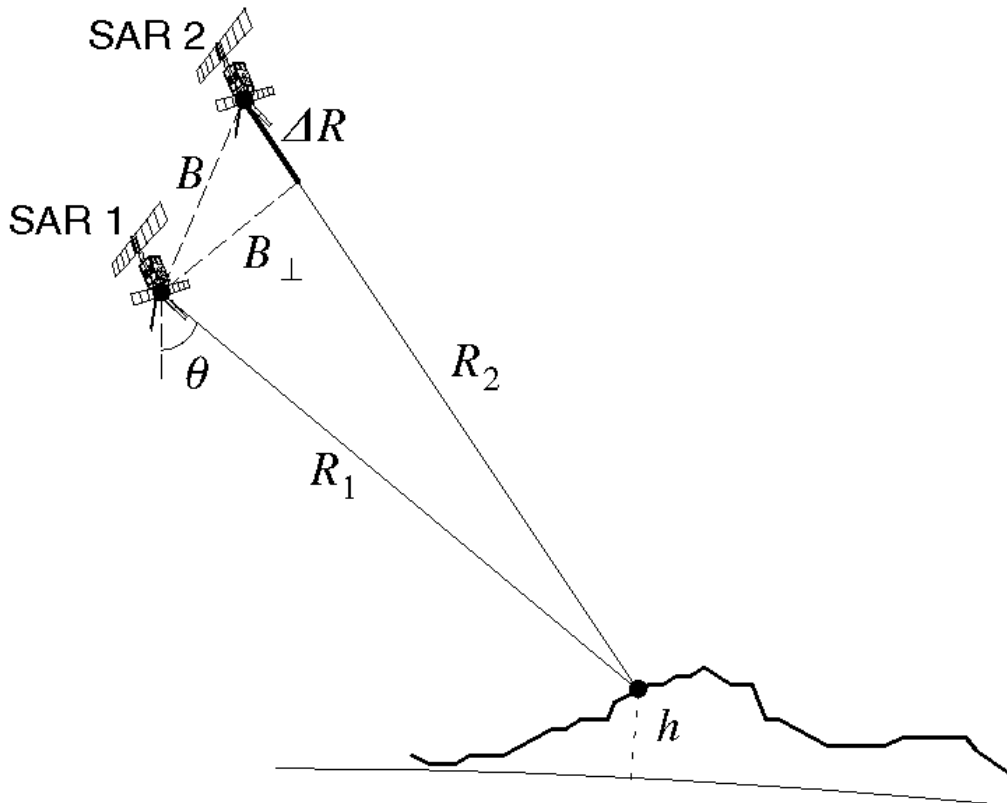


Figure 2: InSAR configuration (flight paths of sensors perpendicular to plane).  $B$  is the baseline of the interferometer.

The configuration depicted in Figure 2 is often referred to as *cross-track interferometer* in order to distinguish it from along-track antenna arrangements built for motion measurements ((Bao et al., 1997), (Carande, 1994), (Goldstein et al., 1989), (Goldstein and Zebker, 1987)). Cross-track SAR interferometers come in two flavours: *Single-pass* interferometers record the required two SAR images simultaneously by using a transmit/receive antenna and a secondary receive antenna mounted some distance away. These interferometers are technically limited in baseline extent but are superior due to reasons discussed below. *Repeat-pass* interferometers, on the other hand, use images taken at different times, e.g. separated by days or months. Hence, any spaceborne SAR can be used as an interferometer in this way, although most of them have not been built according to InSAR requirements and are, thus, not optimal for this application, which is especially true for ERS-1/2. Since there is currently no spaceborne single-pass InSAR system, the equations given in this paper refer to the repeat-pass case if not mentioned otherwise.

The height to phase sensitivity of an repeat-pass across-track SAR interferometer is

$$\frac{\partial \Delta \phi}{\partial h} \cong \frac{4 \pi B_{\perp}}{\lambda R \sin \theta} .$$

From that it would be desirable to operate at large baselines. It can be shown, however, that with increasing baseline the two complex SAR images forming the interferogram tend to decorrelate ((Zebker and Villasenor, 1992), (Zebker et al., 1994)), requiring the so-called spectral shift filtering (Gatelli et al., 1994). Once the spectral shift exceeds the SAR system bandwidth  $W$  the interferogram is completely decorrelated and useless for terrain reconstruction. The maximum allowable baseline is often referred to as the *critical baseline*:

$$B_{\perp, crit} = \frac{\lambda W R \tan(\theta - \alpha)}{c}$$

where  $\alpha$  is the component of the local terrain slope in the range direction and  $c$  is the velocity of light. For ERS-1/2 the critical baseline is about 1050 m.

### 3.1 Example

The following example illustrates both the InSAR processing steps and the information contained in SAR interferograms. Figure 3 shows the magnitude (radar brightness) of a small portion of an ERS image of the Californian Mojave Desert (close to Ft. Irwin). Two of these images taken at a baseline of about 180 m are first co-registered to an accuracy of about 1/10 of pixel and then multiplied to form an interferogram. The interferometric phase is ambiguous with respect to integer multiples of  $2\pi$  and is usually displayed in a colour-wheel fashion. Figure 4 shows the phase in black (0 deg.) and white ( $2\pi$ ), (after removal of an inherent dominant phase trend). The iso-phase lines are usually referred to as fringes and resemble iso-height lines of the terrain. It is, however, not before a 2-D phase unwrapping step removes the  $2\pi$ -phase ambiguity that geolocation of every interferogram pixel can be carried out to generate the DEM (Figure 5). For the practical aspects of InSAR processing see, e.g., Geudtner (1995), Schwäbisch (1995). It should be noted, that phase information is present in every interferogram pixel - even in completely homogeneous areas where classical contrast based stereo methods fail.

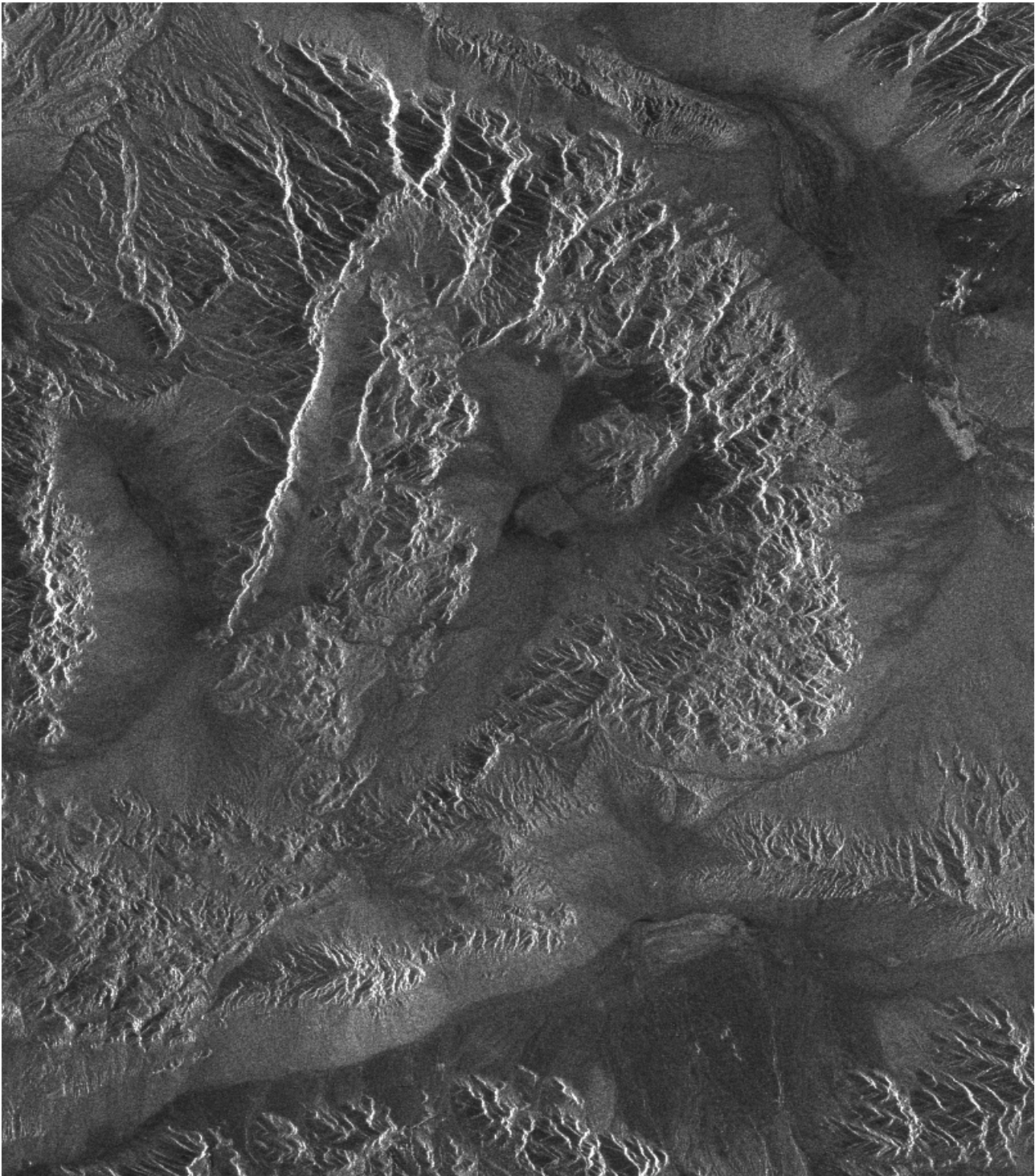


Figure 3: Magnitude ERS SAR image of Mojave Desert, CA, USA. Size  $\approx 40\text{km} \times 40\text{km}$  (data  $\copyright$  ESA).

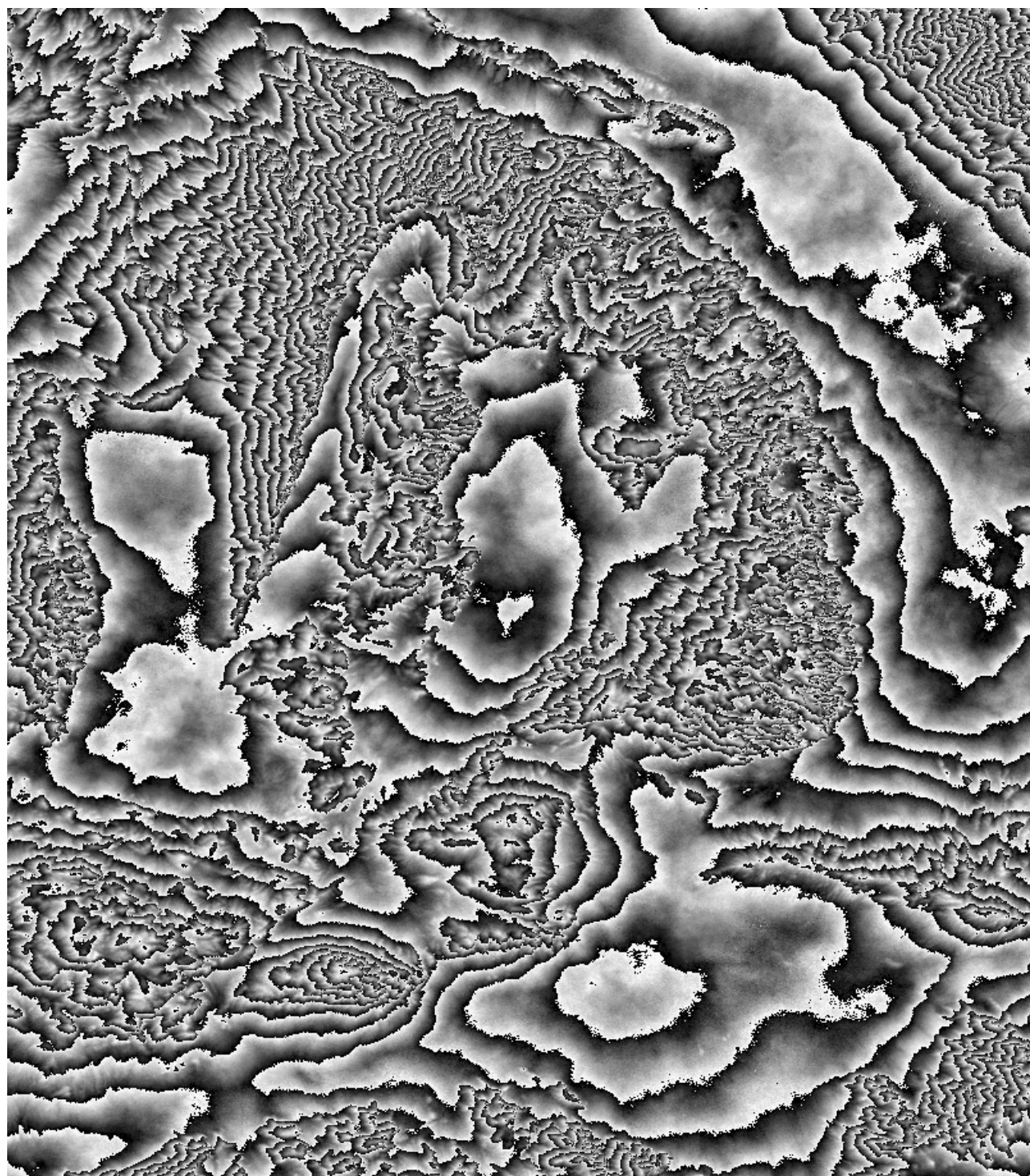


Figure 4: Interferometric fringes of Ft. Irwin scene.

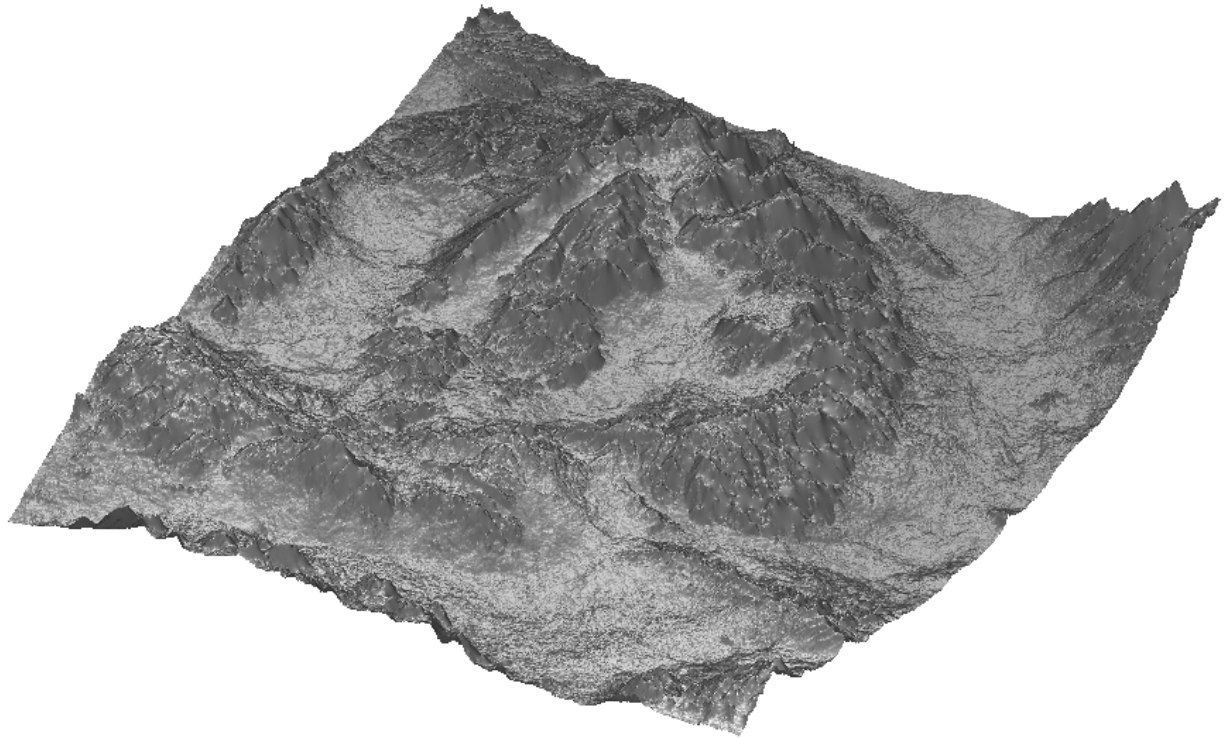


Figure 5: Reconstructed Ft. Irwin DTM (not geocoded).

#### 4. InSAR DTM ACCURACY

The accuracy of an interferometrically generated DTM is determined by these three factors:

1. Measurement accuracy of the phase of a pixel  $\Leftarrow$  phase noise
2. Accuracy of the imaging geometry  $\Leftarrow$  orbit errors
3. Constancy of the wave propagation conditions  $\Leftarrow$  atmospheric artefacts

##### 4.1 Phase Accuracy

Phase noise  $\sigma_{\Delta\phi}$  in the interferogram results in a height error of

$$\sigma_h \cong \frac{\partial h}{\partial \Delta\phi} \sigma_{\Delta\phi} \cong \frac{\lambda R \sin \theta}{4\pi B_{\perp}} \sigma_{\Delta\phi}$$

For example an interferometric ERS configuration with a baseline of 200 m results in  $\sigma_h \cong 0.13$  m per degree phase noise. This type of error varies relatively rapidly from pixel to pixel, i.e. has a short correlation length.

Phase noise originates from different sources, the dominant ones being:

1. *System noise*, e.g. thermal receiver noise and quantization noise: These are the dominant noise sources in single-pass interferometry.
2. *Temporal scene decorrelation*: In repeat-pass interferometry the sub-resolution properties of the imaged scatterer may change between surveys, e.g. by movement of leaves and branches, water

surfaces, or vegetation growth. If the movement of individual sub-scatterers in a resolution cell is in the order of a wavelength, the scattering phase contributions  $\phi_{pscatt,1,2}$  in the two images no longer cancel and the two SAR images decorrelate.

Any source of phase noise can be characterised by the amount of decorrelation it introduces. A commonly used measure for the interferogram quality is *coherence*  $\gamma$  defined as the mutual correlation coefficient between the two images ((Just and Bamler, 1994), (Wegmüller et al., 1995), (Zebker and Villasenor, 1992)). Its magnitude is bounded between 0 (implying total decorrelation, no phase information) and 1 (no phase noise). Phase noise can be reduced by spatially low-pass filtering the interferogram at the expense of horizontal resolution. Figure 6 shows the dependence of phase noise and height error on coherence and resolution for a 200 m baseline ERS-type interferometer.

With modern SAR systems coherence values of  $\gamma > 0.9$  can be easily reached in single-pass mode. Repeat-pass interferometers, on the other hand, suffer from loss of coherence due to temporal scene decorrelation; coherence may take on any value between 0 (water surfaces) and about 0.9 (dry soil, rock). From that we can conclude that with ERS-1/2 height accuracies in the 5 m regime are achievable, if low coherence areas and rugged terrain are excluded ((Prati and Rocca, 1990), (Prati et al., 1989), (Zebker et al., 1994)). This is especially true for data from the dedicated ERS tandem phase, where ERS-1 and ERS-2 were used to acquire interferometric image pairs at a time lag of only 1 day.

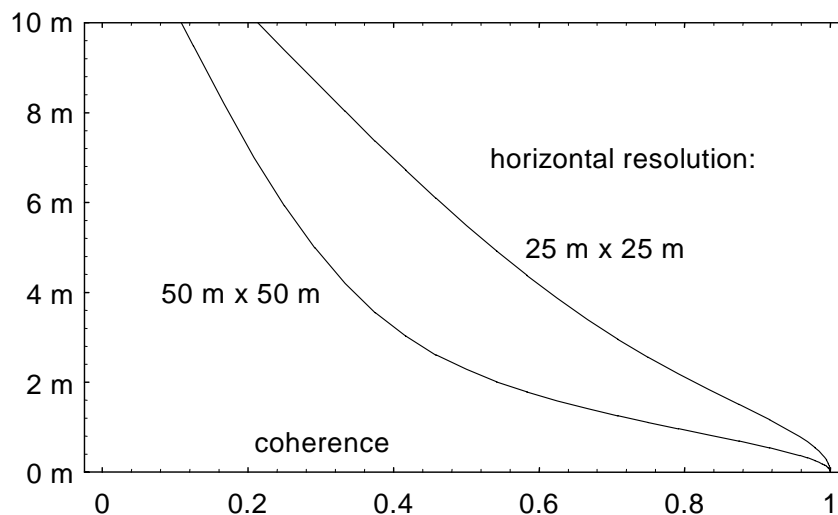


Figure 6: Phase noise induced height error as a function of coherence and horizontal resolution for ERS, baseline 200 m.

## 4.2 Orbit Accuracy

Insufficient accuracy in the sensor position gives rise to smooth large-scale terrain reconstruction errors. From Figure 2 it is obvious that, for example, a horizontal or vertical shift of the entire interferometer by a certain amount will result in the same shift of the reconstructed terrain. An orbit error component that effectively rotates the interferometer baseline will also rotate the DTM. Hence, to first order, orbit errors lead to horizontal and vertical shifts of the entire DTM as well as to ramp-like height distortions. These distortions become more significant with increasing swath width.

The standard approach is using flat areas of known elevation, ground control points, or sea shores as references to improve the baseline and orbit parameters. The problem of inaccurate orbit and attitude is not specific to InSAR, it is rather a geometric one and is similarly encountered in optical imaging. The orbit errors of current spaceborne SARs are in the order of tens of centimetres (ERS), They are still too high for fully automated DTM generation and ground control points are still required.

### 4.3 Propagation Effects

Due to the availability of huge amounts of InSAR data and the increasing throughput of the processing systems propagation effects on interferometric phase can be studied to a greater extent. Repeat-pass interferometry relies on the constancy of the wave propagation conditions for the two acquisitions. Several phenomena are currently blamed to introduce phase delay errors ((Dupont, 1996), (Hanssen and Usai, 1996), (Massonnet et al., 1995)):

1. *Tropospheric water vapour* may cause phase shifts in ERS interferograms. In a high percentage of data sets cloud-like or ripple-like phase structures can be found. The amount of phase error is most often much smaller than 0.5 fringe cycles. Often, this kind of error can be averaged out, since several interferograms of the same area are usually required for DTM generation, anyway.
2. In a small fraction of SAR data localised phase errors due to *convective cells of water vapour* have been observed. Their extent are less than 30 km; the phase error can be 1 ... 3 fringes. Their special structure allows to identify them easily and discard these areas from the interferogram.
3. The influence of the *ionosphere* is not yet well understood. Ionospheric waves are often triggered in arctic regions and propagate to lower latitudes.

## 5. SPACEBORNE SENSORS AND MISSIONS

Until today there is no dedicated SAR interferometer in space. As mentioned above, the poor man's interferometer exploits existing SARs in a repeat-pass fashion. As far as orbit accuracy, coverage, and data availability is concerned the ERS systems seem quite suited for interferometry. ESA operated ERS-1/2 in the 1-day revisit 'tandem' phase to support InSAR applications in 1995 and 1996 for several months. The acquired data cover a good portion of the Earth and, in fact, exhibit considerably better scene coherence than the usual 35 day data. Unfortunately, ERS is quite inflexible with respect to resolution, swath width and incidence angle (Table 1). Particularly its incidence angle is too small for reconstruction of rugged terrain.

Future SARs will offer a suite of favourable imaging modes including the so-called ScanSAR mode which allows for wide swath mapping. The first of this new sensor generation is the Canadian Radarsat, launched in 1996.

### 5.1 Shuttle Radar Topography Mapper

A new era for InSAR will begin with the *Shuttle Radar Topography Mapper (SRTM)* to be launched in 1999 (Jordan et al., 1996). It is a dedicated InSAR mission, flown by NASA on the space shuttle for ten days. The result will be a consistent homogeneous DTM of 80% of the land mass (=  $\pm 60$  deg latitude) at DTED2 quality.

The radar instruments are inherited from the successful SIR-C/X-SAR missions in 1994 augmented by a 60m boom carrying C-band and X-band receive antennas (Figure 7). Together with the primary transmit/receive systems in the shuttle cargo bay they form two interferometers. The C-band system will be supplied by NASA/JPL while the X-band interferometer is a German instrument.

The X-band data will be processed at DLR, Oberpfaffenhofen (Bamler et al., 1996). A SAR processor, an InSAR processing system (*GENESIS*) and a DTM generator (*GEMOS*) are currently developed and implemented at DLR (Eineder and Adam, 1997).

	<b>ERS-1/2</b>	<b>J-ERS</b>	<b>Radarsat</b>	<b>SRTM</b>	<b>Envisat</b>
<b>wavelength</b>	C	L	C	<b>C and X</b>	C
<b>repeat/single pass</b>	repeat	repeat	repeat	<b>single</b>	repeat
<b>repeat cycle</b>	3 or 35 d <b>tandem: 1 d</b>	44 d	24 d	<b>N/A.</b>	35 d (TBD)
<b>global coverage</b>	+	+	++	+	++
<b>orbit accuracy</b>	+	-	-	++	+
<b>incidence angle</b>	23 deg	40 deg	10 - 60 deg	<b>20 - 60 deg</b>	13 - 39 deg
<b>resolution</b>	25 m	25 m	10 m - 100 m	<b>30 m</b>	30 - 1 km
<b>swath width</b>	100 km	100 km	max. 500 km	<b>225 km</b>	100 - 400 km
<b>ScanSAR option</b>	no	no	yes	<b>yes</b>	yes
<b>p r e s e n t</b>				<b>f u t u r e</b>	

Table 1: Current and future spaceborne SARs and InSAR systems (the Russian ALMAZ is not included, since its data are not easily available).

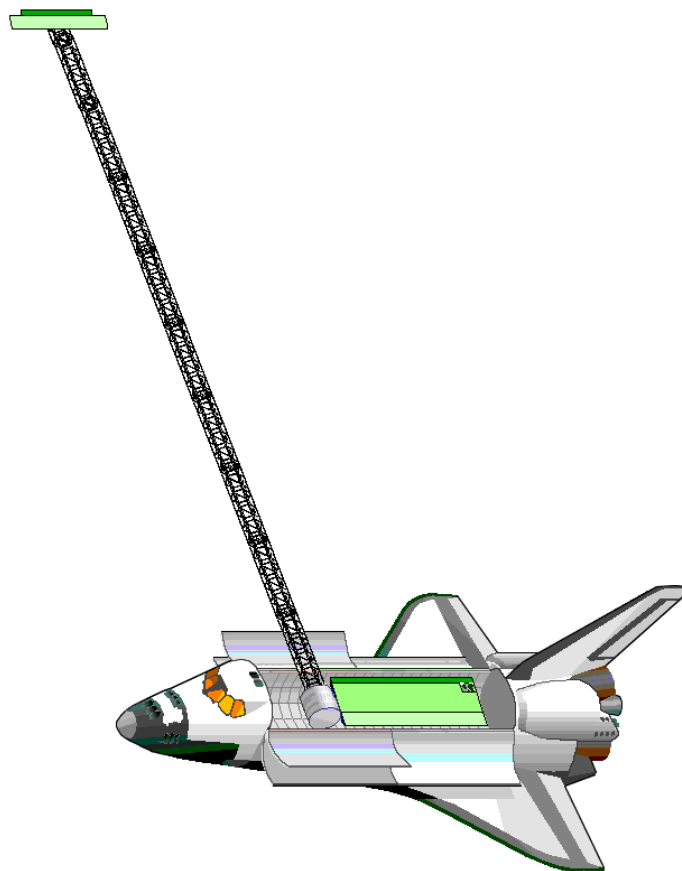


Figure 7: The SRTM space segment.

## 6. CONCLUSIONS

Synthetic aperture radar interferometry is a technology that has been migrating from research labs to applications and operational systems for the recent few years. Compared to optical stereo mapping InSAR is a relatively young method. Although there are several airborne SAR interferometers in operation (e.g. in USA, Canada, Germany, Denmark) that provide high resolution DTMs on a local scale, there is a definite lack of a dedicated spaceborne system for global monitoring so far. SRTM will be the first of that kind.

It should be noted that SAR interferometers are not only useful for DTM generation. Their potential to measure range differences to within an accuracy of centimetres or even millimetres can be exploited to detect tiny deformations and displacements of parts of the Earth's surface (differential InSAR, D-InSAR). Typical applications are monitoring of glacier movement, earthquakes, tectonic and volcanic activities, land sliding, soil erosion ((Gabriel et al., 1989), (Hartl et al., 1994a), (Massonnet et al., 1995), (Massonnet and Rabaute, 1993), (Massonnet et al., 1993), (Zebker and Rosen, 1994)).

## 7. REFERENCES

- Bamler, R., Eineder, M. and Breit, H.: The X-SAR single-pass interferometer on SRTM: Expected performance and processing concept. EUSAR'96, Königswinter, Germany, pp. 181-184.
- Bamler, R. and Schättler, B. (1993): SAR data acquisition and image formation. SAR geocoding: data and systems, G. Schreier, ed., Wichmann, Karlsruhe, pp. 53-102.
- Bao, M., Brüning, C. and Alpers, W. (1997): Simulation of ocean waves imaging by an along-track interferometric synthetic aperture radar. IEEE Transactions on Geoscience and Remote Sensing, 35(3), pp. 618-631.
- Carande, R. E. (1994): Estimating ocean coherence time using dual-baseline interferometric synthetic aperture radar. IEEE Transactions on Geoscience and Remote Sensing, 32(4), pp. 846-854.
- Curlander, J. C. and McDonough, R. N. (1991): Synthetic aperture radar: Systems and signal processing, John Wiley & Sons, New York.
- Dupont, S.: Atmospheric artifacts in SAR interferometry. 3rd ERS Symposium, Florence, Italy.
- Eineder, M. and Adam, N. (1997): A flexible system for the generation of interferometric SAR products. International Geoscience and Remote Sensing Symposium IGARSS'97, Singapore.
- Elachi, C. (1991): Spaceborne imaging radars. International Journal of Imaging Systems and Technology, 3, pp. 167-185.
- Gabriel, A. K. and Goldstein, R. M. (1988): Crossed orbit interferometry: theory and experimental results from SIR-B. International Journal of Remote Sensing, 9(5), pp. 857-872.
- Gabriel, A. K., Goldstein, R. M. and Zebker, H. A. (1989): Mapping small elevation changes over large areas: differential radar interferometry. Journal of Geophysical Research, 94(B 7), pp. 9183-9191.
- Gatelli, F., Monti Guarnieri, A., Parizzi, F., Pasquali, P., Prati, C. and Rocca, F. (1994): The wavenumber shift in SAR interferometry. IEEE Transactions on Geoscience and Remote Sensing, 32(4), pp. 855-865.
- Geudtner, D. (1995): Die interferometrische Verarbeitung von SAR-Daten des ERS-1. 95-28, DLR, Oberpfaffenhofen.
- Goldstein, R. M., Barnett, T. P. and Zebker, H. A. (1989): Remote sensing of ocean current. Science, 246, pp. 1282-1285.
- Goldstein, R. M. and Zebker, H. A. (1987): Interferometric radar measurement of ocean surface current. Nature, 328(6132), pp. 707-709.
- Graham, L. C. (1974): Synthetic interferometer radar for topographic mapping. Proceedings of the IEEE, 62(6), pp. 763-768.

- Hanssen, R. and Usai, S.: Interferometric phase analysis for monitoring slow deformation processes. 3rd ERS Workshop, Florence, Italy.
- Harger, R. O. (1970): Synthetic aperture radar systems: Theory and design, Academic Press, New York.
- Hartl, P., Reich, M., Thiel, K.-H. and Xia, Y.: SAR interferometry applying ERS-1: Some preliminary test results. 1st ERS-1 Symposium, Cannes, France, pp. 219-222.
- Hartl, P., Thiel, K.-H. and Wu, X.: Information extraction from ERS-1 SAR data by means of InSAR and D-InSAR techniques in antarctic research. 2nd ERS-1 Symposium, Hamburg, Germany, pp. 697-701.
- Hartl, P., Thiel, K.-H., Wu, X. and Xia, Y.: Practical applications of SAR interferometry: experiences made by the institute of navigation. 2nd ERS-1 Symposium, Hamburg, Germany, pp. 717-722.
- Jordan, R. L., Caro, E. R., Kim, Y., Kobrik, M., Shen, Y. and Stuhr, F. V. (1996): Shuttle radar topography mapper (SRTM). Microwave sensing and synthetic aperture radar, G. Franceschetti, C. J. Oliver, F. S. Rubertone and S. Tajbakhsh, eds., SPIE, Bellingham, pp. 412-422.
- Just, D. and Bamler, R. (1994): Phase statistics of interferograms with applications to synthetic aperture radar. *Applied Optics*, 33(20), pp. 4361-4368.
- Lanari, R., Fornaro, G., Riccio, D., Migliaccio, M., Papathanassiou, K. P., Moreira, J. R., Schwäbisch, M., Dutra, L., Puglisi, G., Franceschetti, G. and Coltelli, M. (1996): Generation of digital elevation models by using SIR-C/X-SAR multifrequency two-pass interferometry: The Etna case study. *IEEE Transactions on Geoscience and Remote Sensing*, 34(5), pp. 1097-1115.
- Massonnet, D., Briole, P. and Arnaud, A. (1995): Deflation of Mount Etna monitored by spaceborne radar interferometry. *Nature*, 375(June), pp. 570.
- Massonnet, D. and Rabaute, T. (1993): Radar interferometry: limits and potential. *IEEE Transactions on Geoscience and Remote Sensing*, 31(2), pp. 455-464.
- Massonnet, D., Rossi, M., Carmona, C., Adragna, F., Peltzer, G., Feigl, K. and Rabaute, T. (1993): The displacement field of the Landers earthquake mapped by radar interferometry. *Nature*, 364, pp. 138-142.
- Moreira, J., Schwäbisch, M., Fornaro, G., Lanari, R., Bamler, R., Just, D., Steinbrecher, U., Breit, H., Eineder, M., Franceschetti, G., Geudtner, D. and Rinkel, H. (1995): X-SAR interferometry: First results. *IEEE Transactions on Geoscience and Remote Sensing*, 33(4), pp. 950-956.
- Prati, C. and Rocca, F. (1990): Limits to the resolution of elevation maps from stereo SAR images. *International Journal of Remote Sensing*, 11(12), pp. 2215-2235.
- Prati, C. and Rocca, F.: Range resolution enhancement with multiple SAR surveys combination. *Int. Geoscience & Remote Sensing Symposium IGARSS'92*, Houston, Texas, pp. 1576-1578.
- Prati, C. and Rocca, F. (1993): Improving slant-range resolution with multiple SAR surveys. *IEEE Transactions on Aerospace and Electronic Systems*, 29(1), pp. 135-144.
- Prati, C., Rocca, F. and Guanieri, A. M. (1989): Effects of speckle and additive noise on the altimetric resolution of interferometric SAR (ISAR) surveys. *Int. Geoscience & Remote Sensing Symposium IGARSS'89*, Vancouver, Canada, pp. 2469-2472.
- Prati, C., Rocca, F., Pasquali, P. and Monte Guarnieri, A. (1994): Measuring volumetric scattering effects with SAR interferometry. *Topography from Space*, Göteborg, Sweden.
- Raney, R. K. (1982a): Processing synthetic aperture radar data. *International Journal of Remote Sensing*, 3(3), pp. 243-257.
- Raney, R. K. (1982b): Review of spaceborne and airborne SAR systems. *Agard Lecture Series*, 182, 11.1-11.20.
- Richman, D. (1971): Three dimensional azimuth-correcting mapping radar. United Technologies Corporation, USA.
- Rodriguez, E. and Martin, J. M. (1992): Theory and design of interferometric synthetic aperture radars. *IEE Proceedings-F*, 139(2), pp. 147-159.

- Schwäbisch, M. (1995): Die SAR-Interferometrie zur Erzeugung digitaler Geländemodelle. Pp. 95-25, DLR, Oberpfaffenhofen.
- Tomiyasu, K. (1978): Tutorial review of synthetic-aperture radar (SAR) with applications to imaging of the ocean surface. *Proceedings of the IEEE*, 66(5), pp. 563-583.
- Wegmüller, U. and Werner, C. L. (1997): Retrieval of vegetation parameters with SAR interferometry. *IEEE Transactions on Geoscience and Remote Sensing*, 35(1), pp. 18-24.
- Wegmüller, U., Werner, C. L., Nüesch, D. and Borgeaud, M. (1995): Forest mapping using ERS repeat-pass SAR interferometry. *ESA Earth Observation Quarterly*(49), pp. 4-7.
- Zebker, H. A. and Goldstein, R. M. (1986): Topographic mapping from interferometric synthetic aperture radar observations. *Journal of Geophysical Research*, 91(B 5), pp. 4993-4999.
- Zebker, H. A. and Rosen, P.: On the derivation of coseismic displacement fields using differential radar interferometry: the Landers earthquake. *Int. Geoscience & Remote Sensing Symposium IGARSS'94*, Pasadena, CA, USA, pp. 286-288.
- Zebker, H. A. and Villasenor, J. (1992): Decorrelation in interferometric radar echoes. *IEEE Transactions on Geoscience and Remote Sensing*, 30(5), pp. 950-959.
- Zebker, H. A., Werner, C. L., Rosen, P. A. and Hensley, S. (1994): Accuracy of topographic maps derived from ERS-1 interferometric radar. *IEEE Transactions on Geoscience and Remote Sensing*, 32(4), pp. 823-836.